Laser and Particle Beams

cambridge.org/lpb

Nuclear diagnosis of the fuel areal density for direct-drive deuterium fuel implosion at the Shenguang-II Upgrade laser facility

Bo Cui[1], Zhiheng Fang[2], Zenghai Dai[1], Hongjie Liu[1], Wei Wang[2], Jiabin Chen[1], Bi Bi[1], Chao Tian[1], Dongxiao Liu[1], Weiwu Wang[1], Lianqiang Shan[1], Feng Lu[1], Gang Li[1], Faqiang Zhang[1], Bo Zhang[1], Zhimeng Zhang[1], Zhigang Deng[1], Shukai He[1], Jian Teng[1], Wei Hong[1], Yuqiu Gu[1] and Baohan Zhang[1]

[1]Science and Technology on Plasma Physics Laboratory, Research Center of Laser Fusion, China Academy of Engineering Physics, Mianyang 621900, China and [2]Shanghai Institute of Laser Plasma, China Academy of Engineering Physics, Shanghai 201800, China

Research Article

Cite this article: Cui B *et al* (2018). Nuclear diagnosis of the fuel areal density for direct-drive deuterium fuel implosion at the Shenguang-II Upgrade laser facility. *Laser and Particle Beams* **36**, 494–501. https://doi.org/10.1017/S026303461800054X

Received: 22 May 2018
Revised: 26 September 2018
Accepted: 6 December 2018

Key words:
Fuel areal density; low afterglow; neutron time-of-flight; scintillator detector; yield-ratio method

Author for correspondence:
Y.Q. Gu and H.J. Liu, Research Center of Laser Fusion, China Academy of Engineering Physics, Mianyang, China, E-mail: yqgu@caep.cn; buyijie@163.com

Abstract

In inertial confinement fusion experiments that involve short-laser pulses such as fast ignition (FI), diagnosis of neutrons is usually very challenging because high-intensity γ rays generated by short-laser pulses would mask the much weaker neutron signal. In this paper, fast-response scintillators with low afterglow and gated microchannel plate photomultiplier tubes are combined to build neutron time-of-flight (nTOF) spectrometers for such experiments. Direct-drive implosion experiments of deuterium-gas-filled capsules were performed at the Shenguang-II Upgrade (SG-II-UP) laser facility to study the compressed fuel areal density ($\langle \rho R \rangle$) and evaluate the performance of such nTOF diagnostics. Two newly developed quenched liquid scintillator detectors and a gated ultrafast plastic scintillator detector were used to measure the secondary DT neutrons and primary DD neutrons, respectively. The secondary neutron signals were clearly discriminated from the γ rays from (n, γ) reactions, and the compressed fuel areal density obtained with the yield-ratio method agrees well with the simulations. Additionally, a small scintillator decay tail and a clear DD neutron signal were observed in an integrated FI experiment as a result of the low afterglow of the oxygen-quenched liquid scintillator.

Introduction

Fast heating of imploded fuel with an ultraintense short-pulse laser is an attractive approach to realize controllable nuclear fusion (Tabak *et al*., 1994; Solodov *et al*., 2009; Gu *et al*., 2013), which is called fast ignition (FI). Recently developed petawatt (PW) laser systems have realized this scheme in experiments (Theoobald *et al*., 2011; Azechi *et al*., 2013; Shiraga *et al*., 2014). In this scheme, the fuel is first compressed to high areal density with nanosecond (ns)-laser beams ($\sim 10^{15}$ W/cm^2), and then the core of the imploded plasma is heated by a relativistic electron beam generated by a high-power picosecond (ps)-laser beam ($\sim 10^{19}$ W/cm^2). However, the ps laser produces a large amount of γ rays simultaneously, and these γ rays strongly interfere with instruments used to detect neutrons. Neutron diagnosis plays an important role in identifying the status of the confined plasma (Habara *et al*., 2006; Shan *et al*., 2018) because the complex electromagnetic fields in the plasma do not interfere with the flight of neutrons; thus, such techniques provide hot-spot information. Neutron time-of-flight (nTOF) spectrometry employing a fast organic scintillator is a common method to diagnose the neutron yield, fuel areal density and plasma temperature in laser fusion experiments (Stoeckl *et al*., 2010; Forrest *et al*., 2012). Unfortunately, such scintillators also respond to γ rays, making neutron detection challenging in FI because of the strong γ-ray background generated through Bremsstrahlung processes of ∼MeV fast electrons.

There are several methods to alleviate this problem. First, the gamma background can be reduced with a suitable lead shield. Second, the response of the scintillator detector to the gamma burst can be suppressed with adequate gating techniques of the photomultiplier tube (PMT). Unfortunately, these two methods are not sufficient, as the high-intensity gamma flash still masks the much weaker neutron signals (Lauck *et al*., 2009) in experiments. The reason is the long decay time of fluorescence called "afterglow" in conventional organic scintillators, which overwhelms the neutron signals.

Hence, fast organic scintillators with much shorter afterglows are important for inertial confinement fusion (ICF) experiments with strong gamma backgrounds. The oxygen-enriched liquid scintillator (Lauck *et al*., 2009; Stoeckl *et al*., 2010) with a ternary mixture of *p*-xylene as the solvent and 2,5-diphenyloxazole (PPO) and bis(*o*-methylstyryl)-benzene (bis-MSB)

CAMBRIDGE UNIVERSITY PRESS

as fluors is known to provide a fast response and negligible afterglow. Dissolved molecular oxygen is an effective quencher of the triplet excited states in the fluor, which are primarily responsible for the afterglow. Benzophenone, another satisfactory quenching agent, can be doped into the plastic scintillator EJ-232 to obtain the EJ-232Q configuration (Eljen, 2013), achieving better timing performance. To detect the relatively weak neutron signals, the gamma-induced lights in the scintillators need to decay for at least four orders of magnitude in approximately 100 ns.

In this paper, fast-response scintillators with low afterglows are used to build nTOF detectors in a laser direct-drive deuterium fuel implosion experiment. The experiment was performed at the Shenguang-II Upgrade (SG-II-UP) laser facility (Gao *et al.*, 2013; Zhu *et al.*, 2017) to study the compressed fuel areal density and evaluate the performance of nTOF diagnostics. The SG-II-UP facility was designed for ICF and high-energy-density physics experiments, particularly FI research (Cai *et al.*, 2014). The facility delivers eight long-pulse ns-laser beams (in total 24 kJ/3ω/3 ns) for compression and a 1 kJ/1ω/(2–10) ps PW beam for hot electron generation.

In the first stage of FI, the imploded fuel (Stoeckl *et al.*, 2005) can be divided into two regions: one is the hot spot at the center with relatively high temperature and low density, and the other is the cooler fuel region with relatively lower temperature and higher density surrounding the hot spot (Cable and Hatchett, 1987; Rinderknecht *et al.*, 2015). In the implosion of pure-deuterium fuel, ^{3}He and T, the primary fusion products, can traverse the entire hot spot and interact with cooler deuterons (secondary fusion reactions). The probability of a reaction between the primary fusion products and the deuterium fuel is closely related to the areal density $\langle \rho R \rangle$, one of the most important parameters that directly reflects the extent of compression and strongly influences the fuel burn-up fraction.

In low-areal-density pure-deuterium fuel experiments, tritons produced in the primary fusion processes lose negligible energy in the fuel region; hence, the yield ratio of secondary to primary neutrons is approximately proportional to $\langle \rho R \rangle$. The method to determine $\langle \rho R \rangle$ by measuring the yield ratio of the secondary to primary neutrons is called the yield-ratio method and has been applied to experiments with $\langle \rho R \rangle$ below 30 mg/cm^2 (Azechi *et al.*, 1986; Séguin *et al.*, 2002). The secondary neutron yield is several orders of magnitude lower than the primary-neutron yield, so it is challenging to accurately measure the secondary DT neutrons and the primary DD neutrons simultaneously. Here, we use newly developed liquid scintillator detectors (Cui *et al.*, 2016) with a fast response and a gated ultrafast plastic scintillator detector to measure the DT neutrons and DD neutrons, respectively. The γ rays produced through (n, γ) processes inside the target chamber and the chamber wall may overlap with the DT neutron signal; thus, the deployment of neutron detectors is critical.

Yield-ratio method

The fuel areal density $\langle \rho R \rangle$ is defined as the product of the fuel mass density and the spherical fuel radius (Azechi *et al.*, 1986):

$$\langle \rho R \rangle = \int_0^R \rho(r) dr \tag{1}$$

The brackets $\langle\ \rangle$ designate the average over the burn time. The "hot-spot" model (Cable and Hatchett, 1987) assumes that all primary fusion reactions take place in the hot-spot region (whose volume is negligible) and that all secondary fusion reactions take place in a cooler fuel region with uniform density and temperature.

The primary fusion reactions are as follows:

$$\mathrm{D} + \mathrm{D} \rightarrow \mathrm{n}(2.45\ \mathrm{MeV}) + {}^3\mathrm{He}\,(0.82\ \mathrm{MeV}), \tag{2}$$

$$\mathrm{D} + \mathrm{D} \rightarrow \mathrm{p}\,(3.02\ \mathrm{MeV}) + \mathrm{T}\,(1.01\ \mathrm{MeV}). \tag{3}$$

Produced tritons can further react with deuterons (Séguin *et al.*, 2002):

$$\mathrm{T}\,(\leq 1.01\ \mathrm{MeV}) + \mathrm{D} \rightarrow \mathrm{n}'\,(11.9 - 17.2\ \mathrm{MeV}) + {}^4\mathrm{He}. \tag{4}$$

The secondary neutron yield Y_{DT} is typically a few orders lower than the primary neutron yield Y_{DD}, and the ratio $Y_{\mathrm{DT}}/Y_{\mathrm{DD}}$ can be used to infer the value of $\langle \rho R \rangle$ according to the "hot-spot" model. As mentioned above, when $\langle \rho R \rangle$ is low (<30 mg/cm^2), it is a satisfactory approximation to assume that primary-fusion-produced T nuclei lose negligible energy before reacting with deuterons, and the energy-dependent DT reaction cross-section σ can hence be regarded as a constant of $\sigma = 0.4b$. From reactions (2)–(4), the secondary neutron yield Y_{DT} is proportional to the triton yield and the fuel areal density. Hence, the ratio is (Blue and Harris, 1981).

$$\frac{Y_{\mathrm{DT}}}{Y_{\mathrm{DD}}} = \frac{3\sigma}{4\gamma m_{\mathrm{D}}} \langle \rho R \rangle\ [\mathrm{in\ g/cm^2}], \tag{5}$$

where $m_D = 3.34 \times 10^{-24}$ g is the mass of a deuteron, $\sigma = 0.4 \times 10^{-24}$ cm^2, and $\gamma = \langle \sigma v \rangle_{\mathrm{DDN}} / \langle \sigma v \rangle_{\mathrm{DDP}}$ is the ratio of the reaction rate of the D–D neutron branch to that of the proton branch. The value of γ depends on the ion temperature (Hicks, 1999), and in our case, $\gamma = 0.93 \times (1 \pm 0.1)$ since the ion temperature ranges from 1 to 5 keV in our experiments. Equation (5) then becomes

$$\frac{Y_{\mathrm{DT}}}{Y_{\mathrm{DD}}} = 0.096 \langle \rho R \rangle\ [\mathrm{in\ g/cm^2}]. \tag{6}$$

This relation is based on the assumptions that the density and the temperature are spatially uniform, that the reaction time is much shorter than the hydrodynamic time scale, and that the fuel radius is much shorter than the triton free path.

From Eq. (6), the areal density $\langle \rho R \rangle$ can be easily obtained when the yield ratio of DT neutrons to DD neutrons is measured. Since the number of secondary DT neutrons is much less than that of primary DD neutrons, the design and deployment of neutron detectors is essential for obtaining accurate yields of the DT and DD neutrons with a sufficient signal-to-noise ratio.

Experimental configuration

The experiment was performed at the SG-II-UP laser facility with eight long-pulse (ns) laser beams at the National Laboratory on High-power Lasers and Physics, Shanghai. The targets were D_2-filled glass microballoons with a thin SiO_2 coating as the ablator. The capsule had an outer diameter of 450 μm and a wall thickness of 2 μm and was filled with D_2 gas to 15 atm.

https://doi.org/10.1017/S026303461800054X Published online by Cambridge University Press

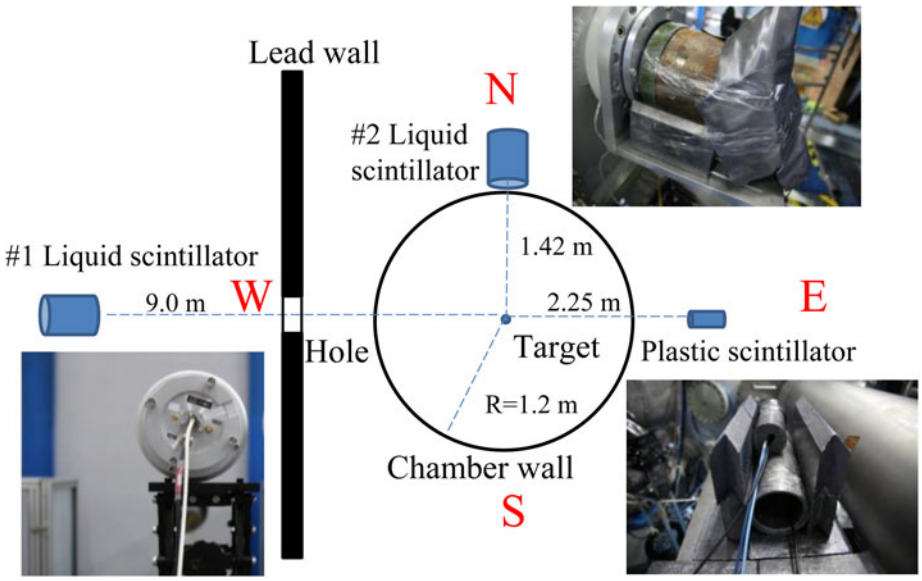

Fig. 1. Configuration of the neutron detectors.

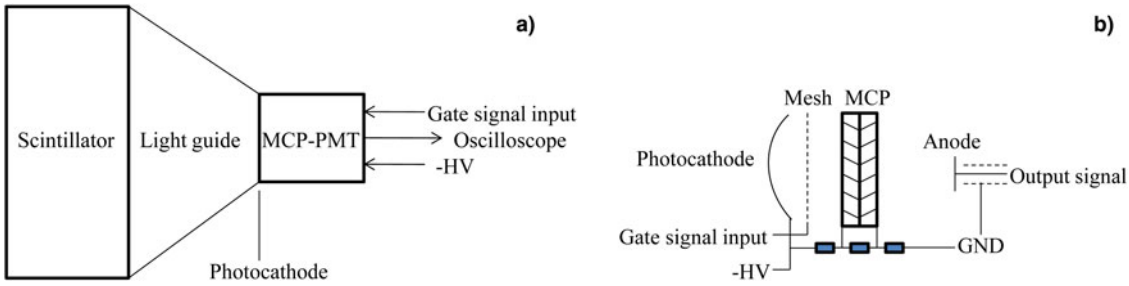

Fig. 2. Schematic diagram of the nTOF detector: (a) configuration of the scintillator detector and (b) simplified electrical schematic of the gated MCP-PMT.

The capsule was irradiated by eight symmetrically pointed beams, delivering 8 kJ of energy in a 1 ns square pulse at 3ω (351 nm).

The main diagnostic equipment of this experiment included nTOF detectors, which were biased at negative high voltages for the measurement of the DT and DD neutrons. Two liquid scintillator neutron detectors and a plastic scintillator neutron detector were used. As shown in Figure 1, the #1 liquid scintillator detector was placed behind a lead wall, and the particles passed into the detector through the hole in the wall; the distance to the target was 9.0 m. The #2 liquid scintillator detector was close to the glass flange of the target chamber, located 1.42 m from the target. To prevent saturation caused by γ rays, the detector was shielded with a lead layer of 3 cm in the front and 1 cm surrounding. The plastic scintillator detector with lower sensitivity was placed in a 1 cm thick lead pig located 2.25 m from the target in the eastward direction as shown in the figure. The inner radius of the vacuum chamber is 1.20 m, and its wall thickness is 7 cm.

Each nTOF detector was composed of a scintillator, a light guide and a microchannel plate PMT (MCP-PMT) connected with a digital oscilloscope, as shown in Figure 2(a). The liquid scintillator detector (Cui *et al.*, 2016) consisted of a cylindrical aluminum (Al) housing filled with a 14-cm-diameter, 10-cm-thick volume of liquid scintillator, which was coupled with a Photek PMT240 (Photek, 2013) with high gain (2×10^5–10^6). This liquid scintillator (Lauck *et al.*, 2009; Cui *et al.*, 2016) included a mixture of two fluorescent dyes, PPO and bis-MSB, dissolved in *p*-xylene and saturated with molecular oxygen. Oxygen was used as the quenching agent to suppress the afterglow caused by strong signals. Compared with those of conventional liquid scintillators for fast neutron detection, for example, BC501A (Patronis *et al.*, 2007), this newly developed liquid scintillator has a much shorter decay time (<2 ns) and lower afterglow, which is well suited to our requirements for satisfactory time-of-flight (TOF) resolution of neutrons and γ rays in high-power laser–target interaction experiments.

The plastic scintillator is a 4-cm-diameter, 1-cm-thick volume of EJ232Q scintillator, mixed with 0.5% benzene as the quenching agent. A Hamamatsu gated R5916U MCP-PMT (Hamamatsu, 2014) with a 1-cm-diameter photocathode is coupled to the plastic scintillator with a light guide. The gain of the PMT can be adjusted by changing the biased voltage according to the operational range of the detector.

The MCP-PMT has a smaller volume with faster timing capability and higher current gain than the conventional PMT (Leskovar, 1977). The general structure of the gated MCP-PMT used in this experiment is shown in Figure 2(b). The MCP has a two-stage chevron configuration, and there is a mesh gate between the photocathode and the MCP that becomes inactive when a positive pulse is applied to the gate. When the MCP-PMT is gated off, the photoelectrons from the photocathode cannot reach the MCP, and this configuration can be used to reduce the amplitude of the large background significantly.

https://doi.org/10.1017/S026303461800054X Published online by Cambridge University Press

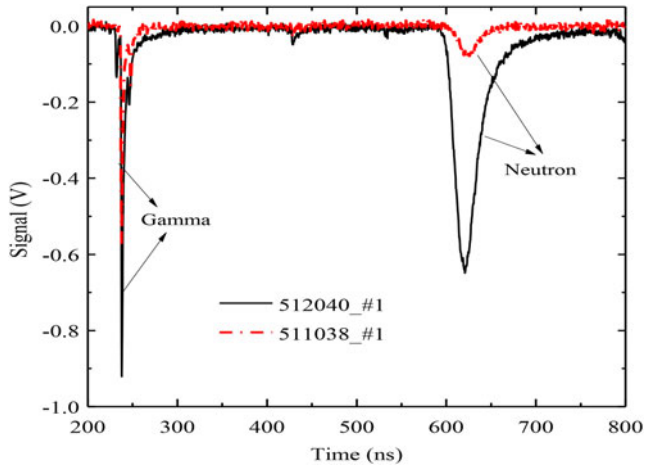

Fig. 3. Typical signals obtained by the #1 liquid scintillator detector.

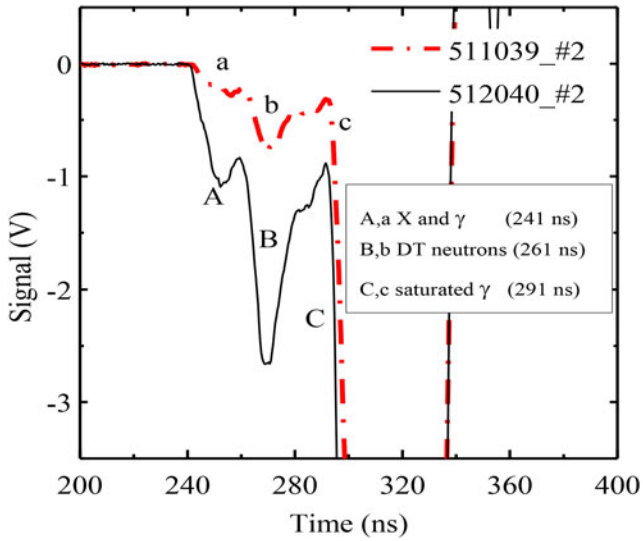

Fig. 4. Secondary DT neutron signals obtained by the #2 liquid scintillator detector.

The time for gating can be adjusted by an induction gate controller and a delayed signal generator.

The sensitivities of the liquid scintillator detectors and the plastic scintillator detector biased at various voltages were calibrated with a compact dense plasma focus (DPF) neutron source (Burns *et al.*, 1989; Geng, 2007) and a 400-keV electrostatic accelerator (K-400) neutron source (Ruiz *et al.*, 1992, 2012; Wu *et al.*, 2006) at the Institute of Nuclear Physics and Chemistry, China Academy of Engineering Physics. The uncertainty of the calibration using the DPF neutron source includes the fluctuations of statistical counting, the reading error of the neutron signal integral area, the source-to-detector distance, etc. The uncertainty in the calibration using the K-400 accelerator neutron source includes the scattered neutron background of the accelerator room, the solid angle of the detector, neutron yield monitoring (Zhu *et al.*, 2007), the γ-ray net counts, etc. The two kinds of calibration results are in agreement with each other. The errors on the sensitivity of DD and DT neutrons were 7 and 20%, respectively. The latter was much larger because the corresponding neutron source adopted for calibration was much weaker.

Experimental results and discussion

A typical signal obtained with the #1 liquid scintillator detector is shown in Figure 3. The peak time of the γ-ray signal is located at $t = 238$ ns, and the peak time of the neutron signal is at $t = 621$ ns. The distance from the #1 liquid scintillator detector to the target chamber center is 9 m, and this neutron signal corresponds to the primary DD neutrons according to the TOF method (Lerche and Remington, 1990), that is, $t = 72.3l/\sqrt{E_n}$, where t is the neutron flight time (in ns), l is the distance from the target to the detector (in m) and E_n is the neutron energy (in MeV). Since the DT neutron yield is several orders lower than the DD neutron yield (Blue and Harris, 1981), the DT neutron signal is too weak for detector #1 to acquire.

Typical signals obtained with the #2 liquid scintillator detector are shown in Figure 4. According to the velocity of various products created by the laser–target interaction, the earliest arrived are the X rays (Azechi *et al.*, 1986; Glebov *et al.*, 2001), which come at $t = 241$ ns. This signal indicates that a lead layer of 3 cm is insufficient to shield all the hard X rays. The next signals are γ-ray signals (A, a), which are due to (n, γ) reactions with the target positioner and diagnostic instruments inside the chamber. Signals (B, b) correspond to DT neutrons, as the maximal energy of the neutron signals is 17.2 MeV (starting at $t = 261$ ns). The saturated signals (C, c) arrive 50 ns later than the X-ray signal, which corresponds to γ rays produced by DD neutrons interacting with the chamber wall. A large number of DD neutrons subsequently arrive and saturate the detector. The fast response of the scintillator and reasonable distance between the detector and the target allowed clear discrimination of the secondary DT neutron signals from the γ-ray signals introduced by DD neutron–chamber wall interaction. In this experiment, this distance should be less than 2.0 m to prevent DD neutron–chamber wall interaction-induced γ rays from masking the secondary DT neutron signals.

The #2 detector was biased at −3200 V, and its sensitivity for DT neutrons was 0.24 ± 0.05 pC/n. The DT neutron yields of shots 511,039 and 512,040 were $(3.3 \pm 1.4) \times 10^5$ and $(1.2 \pm 0.5) \times 10^6$, respectively. The target and laser conditions of these shots were set unchanged, but in shot 512039, a laser beam switch was damaged. Hence, one of the eight ns beams delivered an energy of only 22 J to the capsule, and the spherical compression symmetry was violated. Note that the uncertainty was influenced not only by the uncertainty of the detector sensitivity as described in the section "Experimental configuration" but also by the solid angle, the reading error of neutron signal integral area and the statistical error of the number of detected DT neutrons. Together, these errors compose a total error of ~42%. Applying the gate, the MCP-PMT can be protected from damage induced by the burst of DD neutron signals.

According to glow curves reported previously (Lauck *et al.*, 2009), the signal decays in various types of scintillators are very similar in the first 10–20 ns, and the benefit of the oxygen-enriched liquid scintillator with a ternary mixture of *p*-xylene as the solvent and PPO and bis-MSB as fluors is significant after ~50 ns. The time differences between the γ-ray peaks and the secondary neutron peaks in Figure 4 are <20 ns, so no benefit from the oxygen-quenched liquid scintillator is expected. For high-fuel-areal-density measurements in cryogenic implosions (Izumi *et al.*, 2003; Glebov *et al.*, 2014), these spectrometers are located far enough from the targets (~10 m) to differentiate

https://doi.org/10.1017/S026303461800054X Published online by Cambridge University Press

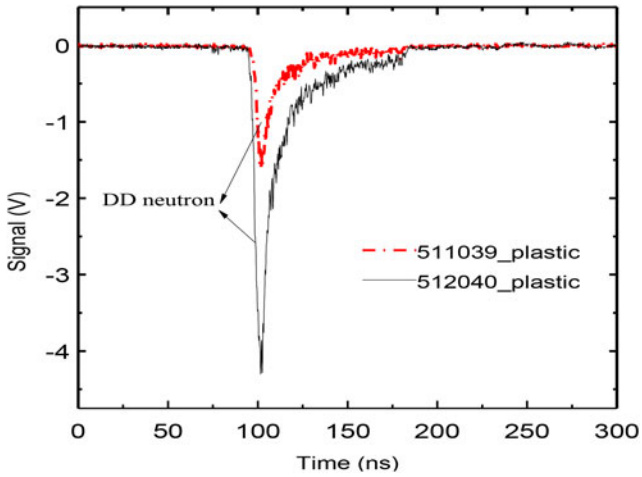

Fig. 5. Primary DD neutron signals obtained by the plastic scintillator detector.

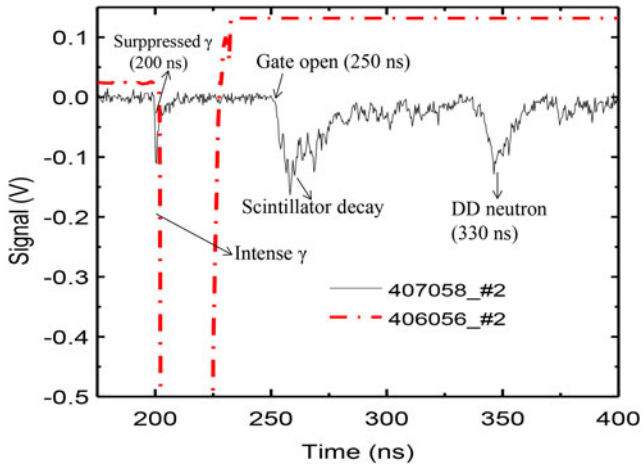

Fig. 6. Signals obtained by the #2 liquid scintillator detector in the integrated FI experiment.

down-scattered neutrons from high primary-neutron backgrounds due to the sufficient resolution of nTOF spectroscopy.

The plastic scintillator detector was coupled to a gated MCP-PMT, and the gate of the PMT was switched on at $t = 75$ ns and switched off at $t = 185$ ns. As displayed in Figure 5, only the primary DD neutron signals were captured. Hard X rays created by the laser–target interaction and γ rays produced by DD neutron interactions with the chamber wall were completely suppressed by the gating. The detector was biased at −2700 V with the gain equal to 2.7×10^4, and its sensitivity for DD neutrons was 0.015 ± 0.001 pC/n. The DD neutron yields of shot 512,039 and shot 512,040 were $(1.65 \pm 0.12) \times 10^9$ and $(4.8 \pm 0.34) \times 10^9$, respectively. The uncertainties were due mainly to the detector calibration and the statistical fluctuations, which were calculated to be ±7%.

By deconvolving the DD nTOF spectrum (Lerche and Remington, 1990; Chen *et al.*, 2001), the ion temperatures were obtained with the formula $T_{\rm ion} = (1.285 \times \Delta t/D)^2$, where $T_{\rm ion}$ is the ion temperature (keV), Δt is the full width at half maximum for the temporal spread of the nTOF spectrum (ns), and D is the distance between the target and the detector (in m). $T_{\rm ion}$ was 1.9 ± 0.3 and 3.4 ± 0.5 keV for the two shots. The uncertainties were determined by the error in the Δt measurement, that is, $\sigma_{\Delta t}$, which was calculated to be 15% with the relations derived by Lerche and Remington (Lerche and Remington, 1990).

The implosion of D_2-filled capsules was driven by the exploding of the glass shell and subsequent hydrodynamic compression of the fuel. In this process, the laser energy deposits in the glass so fast that the shell explodes. Approximately half of the shell mass explodes outward, and the remaining half implodes inward, which drives a shock wave into the fuel (Rosen and Nuckolls, 1979; Ahlborn and Key, 1981; Rosenberg *et al.*, 2014). Both the shock and the imploding pusher shell compress and heat the D_2 gas, creating a "hot spot" at the center of the fuel. The compressed fuel areal density can be obtained with the yield ratio of secondary DT neutrons to primary DD neutrons (i.e., Eq. (6)), and $\langle \rho R \rangle_{\rm fuel}$ for shot 512,039 and shot 512,040 were 1.9 ± 0.9 and 2.4 ± 1.1 mg/cm^2, respectively. The error in $\langle \rho R \rangle_{\rm fuel}$ was a result of DT and DD neutron errors.

The initial mass density of the 15 atm D_2 gas was 2.68 mg/cm^3, and the initial fuel radius ($R_{\rm f0}$) was 0.0223 cm; thus, the initial fuel areal density ($\langle \rho R_{\rm f0} \rangle$) before implosion was 0.06 mg/cm^2. The implosion convergence ratios, that is, the initial fuel radius to the final thermonuclear radius, were 5.6 and 6.3 for the two shots.

Since the experiment described above involves a pure implosion without short-pulse (ps or fs) lasers, the γ-ray background was not very strong. As shown in Figure 4, the signals of background γ rays (B, b) were weaker than the secondary neutron signals, and both were within the linear range of the detector and scope; thus, the advantage of the fast-decaying characteristic of the oxygenated liquid scintillator was not clearly shown. Hence, we further tested the neutron detector in an integrated FI experiment with a ps laser.

The FI experiment was also performed at the SG-II-UP laser facility. A deuterated polystyrene (CD) shell (400 μm inner diameter, 50 μm thickness) with an embedded hollow golden cone was imploded by soft X rays transformed from the eight long-pulse beams (351 nm, 2 ns) with a total energy of 20 kJ ablating the Au hohlraum. A 10-μm CH coating was used to suppress the neutrons generated from the beam–target interaction at the interface of the CD shell and the expanding Au plasma bubbles generated on the hohlraum wall (Shan *et al.*, 2018). At the maximum compression time, a short-pulse laser (1053 nm, 3 ps) with an energy of 150 J was injected into the inner tip of the hollow golden cone to generate fast electrons and then heat the core plasma.

The fast electrons generated a large amount of γ rays through Bremsstrahlung processes. The main diagnostic of the neutron yield was the #2 liquid scintillator detector located 3.0 m from the target, which was shielded with a 10-cm layer of lead in front and 5 cm of surrounding lead. The detector was biased at −3800 V, and its sensitivity for DD neutrons was 1.84 ± 0.13 pC/n. The solid line in Figure 6 is the signal obtained in shot 407058. The γ-ray (200 ns) signal was suitably suppressed by the MCP-PMT gating. The gate was opened at 250 ns, and a small scintillator decay tail was observed that arose from the low afterglow of the oxygenated liquid scintillator. A clear DD neutron signal that started at 330 ns was captured, and the neutron yield was $(7.4 \pm 0.8) \times 10^5$. The uncertainty is due to the error of the sensitivity, the attenuation of lead shielding and the statistical error. When the gate was removed in shot 407,056 (the target and the laser parameter are the same as in shot 407,058), the detector was saturated by intense γ rays.

High-resolution nTOF spectrometers were installed at the SG-II-UP laser facility, providing reliable measurements of the

https://doi.org/10.1017/S026303461800054X Published online by Cambridge University Press

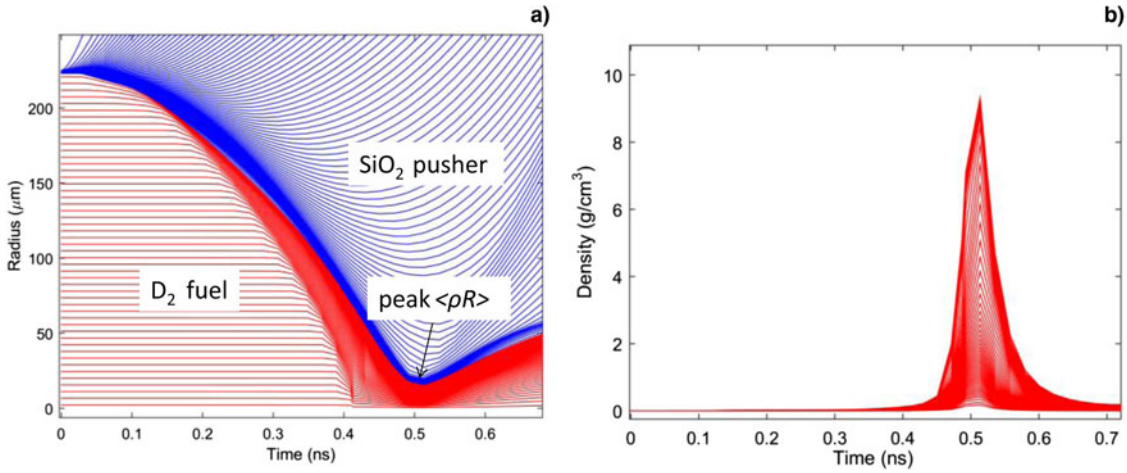

Fig. 7. Multi-1D simulation results: (a) streamlines of the implosion layer and (b) density distribution of D_2 fuel.

neutron yield, ion temperature, compressed fuel areal density, and implosion convergence ratio. These nTOF spectrometers can differentiate the thermonuclear neutrons from the neutrons by beam-fusion, (p, n) and (γ, n) reactions in the experiments with an ultraintense short-pulse laser and can distinguish down-scattered neutrons from strong primary-neutron backgrounds in high-fuel-areal-density cryogenic implosions.

Simulation results and discussion

The hydrodynamic instability and fuel-shell mixing can increase the energy loss of primary-fusion-produced tritons (Séguin *et al.*, 2002; Kurebayashi *et al.*, 2005). If the triton energy is significantly decreased, the cross-section of the DT reaction σ increases and cannot be regarded as a constant. The $\langle \rho R \rangle_{\text{fuel}}$ obtained by the yield ratio method according to Eq. (5) would then be higher than the actual value. To verify the applicability of the yield-ratio method for low-$\langle \rho R \rangle$ implosions, we performed a one-dimensional (1D) hydrodynamic simulation with Multi-1D (Ramis *et al.*, 1988), which is a 1D hydrodynamic software package incorporating coupled thermal radiation transport, heat conduction, and several energy deposition mechanisms: laser beams, ion beams, and fusion-produced α particles.

The direct drive compression of the D_2 gas was simulated in spherical coordinates based on Multi-1D. The laser parameters are as follows: the total energy is 8 kJ, the energy concentration is 50%, $\lambda = 351$ nm, the pulse duration is 1 ns, and the average laser intensity is 6.2×10^{14} W/cm^2. The capsule has an outer diameter of 450 μm and a SiO_2 glass wall of 2 μm and is filled with D_2 gas with a density of 2.68 mg/cm^3.

Multi-1D simulation results are shown in Figure 7. The streamlines of the implosion layer are illustrated in Figure 7(a). The thin SiO_2 shell is ablated away, driving a strong shock wave into the D_2 gas. This shock compresses the D_2, converges at the center and then rebounds. The rebounding shock compresses the gas once again, and a shock-phase is produced. The D_2 fuel reaches peak compression at 0.51 ns, and the minimal compressed fuel radius is 15 μm. The time history of the D_2 fuel density is shown in Figure 7(b), and the maximal density at the peak compression time (0.51 ns) is 9.315 g/cm^3. The simulation prediction for the fuel areal density $\langle \rho R_f \rangle$ is 3 mg/cm^2 at 0.51 ns according to Eq. (1), which is consistent with our experimental result of shot 512,040 (2.4 ± 1.1 mg/cm^2) with the same target and laser parameters, which indicates that the yield-ratio method is suitable for estimating $\langle \rho R \rangle$ for low-fuel-areal-density implosions.

Conclusion

High-resolution nTOF spectrometers have been developed at the SG-II-UP laser facility to measure the neutron yield and areal density of imploded deuterium-filled capsules. Quenched liquid scintillator detectors with a fast response and gated ultrafast plastic scintillator detector were separately deployed at suitable distances to measure the DT and DD neutrons. A clear secondary neutron signal was obtained, and the compressed fuel areal density was obtained with the yield-ratio method, which agrees well with the Multi-1D simulations. The results verify that the yield-ratio method is well suited to estimate $\langle \rho R \rangle$ in low-$\langle \rho R \rangle$ implosion experiments. In an integrated FI experiment with a ps laser having a strong γ-ray background, the gated liquid scintillator detector obtained a clear signal of DD neutrons owing to the low afterglow of the oxygenated liquid scintillator.

Such nTOF spectrometers can be used to diagnose the ion temperature, areal density and confinement time of compressed plasma in FI experiments and can also distinguish the thermonuclear neutrons from the beam-fusion neutrons and the (p, n) and (γ, n) neutrons in experiments with ultraintense short-pulse lasers.

Author ORCIDs. Bo Cui, 0000-0003-0991-3255.

Acknowledgements. The authors gratefully acknowledge the SG-II-UP facility staff for operating the laser facility in the experiment. Bo Cui would like to thank Yuchi Wu for fruitful discussions. This work was supported by the Science Challenge Project (no. TZ2018005) and the National Natural Science Foundation of China (no. 11375159).

References

Ahlborn B and Key MH (1981) Scaling laws for laser driven exploding pusher targets. *Plasma Physics* **23**, 435–447.

Azechi H, Miyanaga N, Stapf RO, Itoga K, Nakaishi H, Yamanaka M, Shiraga H, Tsuji R, Ido S and Nishihara K (1986) Experimental determination of fuel density-radius product of inertial confinement fusion targets using secondary nuclear fusion reactions. *Applied Physics Letters* **49**, 555–557.

https://doi.org/10.1017/S026303461800054X Published online by Cambridge University Press

Azechi H, Mima K, Shiraga S, Fujioka S, Nagatomo H, Johzaki T, Jitsuno T, Key M, Kodama R, Koga M, Kondo K, Kawanaka J, Miyanaga N, Murakami M, Nagai K, Nakai M, Nakamura H, Nakamura T, Nakazato T, Nakao Y, Nishihara K, Nishimura H, Norimatsu T, Norreys P, Ozaki T, Pasley J, Sakagami H, Sakawa Y, Sarukura N, Shigemori K, Shimizu T, Sunahara A, Taguchi T, Tanaka K, Tsubakimoto K, Fujimoto Y, Homma H and Iwamoto A (2013) Present status of fast ignition realization experiment and inertial fusion energy development. *Nuclear Fusion* **53**, 587–593.

Blue TE and Harris DB (1981) Ratio of d-t to d-d reactions as a measure of the fuel density-radius product in initially tritium-free inertial confinement fusion targets. *Nuclear Science and Engineering* **77**, 463–469.

Burns EJT, Falacy SM, Hill RA, Thacher PD, Koehler HA and Davis B (1989) A compact dense-plasma-focus neutron source for detector calibrations. *Nuclear Instruments & Methods in Physics Research, Section B: Beam Interactions with Materials and Atoms* **40–41**, 1248–1251.

Cable MD and Hatchett SP (1987) Neutron spectra from inertial confinement fusion targets for measurement of fuel areal density and charged particle stopping powers. *Journal of Applied Physics* **62**, 2233–2236.

Cai HB, Wu SZ, Wu JF, Mo C, Hua Z, He MQ, Cao LH, Zhou CT, Zhu SP and He XT (2014) Review of the current status of fast ignition research at the IAPCM. *High Power Laser Science and Engineering* **2**, 1–9.

Chen JB, Zheng ZJ, Peng HS, Zhang BH, Ding YK, Chen M, Chen HS and Wen TS (2001) Fusion fuel ion temperatures diagnostic for directly driven implosions. *Review of Scientific Instruments* **72**, 3534–3536.

Cui B, He SK, Liu HJ, Dai ZH, Yan YH, Lu F, Li G, Zhang FQ, Hong W and Gu YQ (2016) Neutron spectrum measurement for picosecond laser pulse neutron source experiment with liquid scintillator detector. *High Power Laser and Particle Beams* **28**, 124005.

Eljen Technology (2013) EJ-232Q data sheet. Sweetwater, TX 79556, USA. http://www.eljentechnology.com

Forrest CJ, Radha PB, Glebov VY, Goncharov VN, Knauer JP, Pruyne A, Romanofsky M, Sangster TC, Shoup III MJ, Stoeckl C, Casey DT, Gatu-Johnson M and Gardner S (2012) High-resolution spectroscopy used to measure inertial confinement fusion neutron spectra on Omega. *Review of Scientific Instruments* **83**, 10D919.

Gao YQ, Ma WX, Cao ZD, Zhu J, Yang XD, Da YP, Zhu BQ and Lin ZQ (2013). Status of the SG-II-UP laser facility. Conference Status of the SG-II-UP laser facility, pp. 73–74.

Geng T (2007) Scintillation neutron detector for DPF device. *High Power Laser and Particle Beams* **19**, 1008–1010.

Glebov VY, Meyerhofer DD, Stoeckl C and Zuegel JD (2001) Secondary-neutron-yield measurements by current-mode detectors. *Review of Scientific Instruments* **72**, 824–827.

Glebov VY, Forrest CJ, Marshall KL, Romanofsky M, Sangster TC, Shoup III MJ and Stoeckl C (2014) A new neutron time-of-flight detector for fuel-areal-density measurements on OMEGA. *Review of Scientific Instruments* **85**, 11E102.

Gu YQ, Yu JQ, Zhou WM, Wu FJ, Wang J, Liu HJ, Cao LF and Zhang BH (2013) Collimation of hot electron beams by external field from magnetic-flux compression. *Laser and Particle Beams* **31**, 579–582.

Habara H, Norreys PA, Kodama R, Stoeckl C and Glebov VY (2006) Neutron measurements and diagnostic developments relevant to fast ignition. *Fusion Science and Technology* **49**, 517–531.

Hamamatsu Photonics KK, Photomultiplier Tube (2014) R5916U data sheet. 1820, Kurematsu, Nishi-ku, Hamamatsu City 431-1202, Japan. http://www.hamamatsu.com.

Hicks DG (1999) Charged-Particle Spectroscopy: A New Window on Inertial Confinement Fusion (Ph.D. thesis). Massachusetts Institute of Technology, Boston.

Izumi N, Lerche RA, Phillips TW, Schmid GJ, Moran MJ, Koch JA, Azechi H and Sangster TC (2003) Development of a gated scintillation fiber neutron detector for areal density measurements of inertial confinement fusion capsules. *Review of Scientific Instruments* **74**, 1722–1725.

Kurebayashi S, Frenje JA, Séguin FH, Rygg JR, Li CK, Petrasso RD, Glebov VY, Delettrez JA, Sangster TC, Meyerhofer DD, Stoeckl C, Soures JM, Amendt PA, Hatchett SP and Turner RE (2005) Using nuclear data and Monte Carlo techniques to study areal density and mix in D_2 implosions. *Physics of Plasmas* **12**, 032703.

Lauck R, Brandis M, Bromberger B, Dangendorf V, Goldberg MB, Mor I, Tittelmeier K and Vartsky D (2009) Low-afterglow, high-refractive-index liquid scintillators for fast-neutron spectrometry and imaging applications. *IEEE Transactions on Nuclear Science* **56**, 989–993.

Lerche RA and Remington BA (1990) Detector distance selection for neutron time-of-flight temperature measurements. *Review of Scientific Instruments* **61**, 3131–3133.

Leskovar B (1977) Microchannel plates. *Physics Today* **30**, 42–49.

Patronis N, Kokkoris M, Giantsoudi D, Perdikakis G, Papadopoulos CT and Vlastou R (2007) Aspects of GEANT4 Monte-Carlo calculations of the BC501A neutron detector. *Nuclear Instruments & Methods in Physics Research, Section A: Accelerators, Spectrometers, Detectors, and Associated Equipment* **578**, 351–355.

Photek Ltd. (2013) PMT240 data sheet. St. Leonards-on-Sea, East Sussex, TN38 9NS, United Kingdom. http://www.photek.co.uk.

Ramis R, Schmalz J and Meyer-ter-Vehn J (1988) MUTLI: a computer code for one-dimensional multigroup radiation hydrodynamics. *Computer Physics Communications* **49**, 475.

Rinderknecht HG, Rosenberg MJ, Zylstra AB, Lahmann B, Séguin FH, Frenje JA, Li CK, Gatu Johnson M, Petrasso RD, Berzak Hopkins LF, Caggiano JA, Divol L, Hartouni EP, Hatarik R, Hatchett SP, Le Pape S, Mackinnon AJ, McNaney JM, Meezan NB, Moran MJ, Bradley PA, Kline JL, Krasheninnikova NS, Kyrala GA, Murphy TJ, Schmitt MJ, Tregillis IL, Batha SH, Knauer JP and Kilkenny JD (2015) Using multiple secondary fusion products to evaluate fuel pR, electron temperature, and mix in deuterium-filled implosions at the NIF. *Physics of Plasmas* **22**, 082709.

Rosen MD and Nuckolls JH (1979) Exploding pusher performance– A theoretical model. *Physics of Fluids* **22**, 1393–1396.

Rosenberg MJ, Zylstra AB, Séguin FH, Rinderknecht HG, Frenje JA, Johnson MG, Sio H, Waugh CJ, Sinenian N, Li CK, Petrasso RD, McKenty PW, Hohenberger M, Radha PB, Delettrez JA, Glebov VY, Betti R, Goncharov VN, Knauer JP, Sangster TC, LePape S, Mackinnon AJ, Pino J, McNaney JM, Rygg JR, Amendt PA, Bellei C, Benedetti LR, Hopkins LB, Bionta RM, Casey DT, Divol L, Edwards MJ, Glenn S, Glenzer SH, Hicks DG, Kimbrough JR, Landen OL, Lindl JD, Ma T, MacPhee A, Meezan NB, Moody JD, Moran MJ, Park H-S, Remington BA, Robey H, Rosen MD, Wilks SC, Zacharias RA, Herrmann HW, Hoffman NM, Kyrala GA, Leeper RJ, Olson RE, Kilkenny JD and Nikroo A (2014) Investigation of ion kinetic effects in direct-drive exploding-pusher implosions at the NIF. *Physics of Plasmas* **21**, 122712.

Ruiz CL, Leeper RJ, Schmidlapp FA, Cooper G and Malbrough DJ (1992) Absolute calibration of a total yield indium activation detector for DD and DT neutrons. *Review of Scientific Instruments* **63**, 4889–4991.

Ruiz CL, Chandler GA, Cooper GW, Fehl DL, Hahn KD, Leeper RJ, McWatters BR, Nelson AJ, Smelser RM, Snow CS and Torres JA (2012) Progress in obtaining an absolute calibration of a total deuterium-tritium neutron yield diagnostic based on copper activation. *Review of Scientific Instruments* **83**, 10D913.

Séguin FH, Li CK, Frenje JA, Hicks DG, Green KM, Kurebayashi S, Petrasso RD, Soures JM, Meyerhofer DD, Glebov VY, Soures JM, Meyerhofer DD, Glebov VY, Radha PB, Stoeckl C, Roberts S, Sorce C, Sangster TC, Cable MD, Fletcher K and Padalino S (2002) Using secondary-proton spectra to study the compression and symmetry of deuterium-filled capsules at OMEGA. *Physics of Plasmas* **9**, 2725–2737.

Shan LQ, Cai HB, Zhang WS, Tang Q, Zhang F, Song ZF, Bi B, Ge FJ, Chen JB, Liu DX, Wang WW, Yang ZH, Qi W, Tian C, Yuan ZQ, Zhang B, Yang L, Jiao JL, Cui B, Zhou WM, Cao LF, Zhou CT, Gu YQ, Zhang BH, Zhu SP and He XT (2018) Experimental evidence of kinetic effects in indirect-drive inertial confinement fusion hohlraums. *Physical Review Letters* **120**, 195001.

Shiraga H, Nagatomo H, Theobald W, Solodov AA and Tabak M (2014) Fast ignition integrated experiments and high-point design. *Nuclear Fusion* **54**, 054005.

https://doi.org/10.1017/S026303461800054X Published online by Cambridge University Press

Solodov AA, Anderson KS, Betti R, Betti V, Gotcheva V, Myatt J, Delettrez JA, Skupsky S, Theobald W and Stoeckl C (2009) Integrated simulations of implosion, electron transport, and heating for direct-drive fast-ignition targets. *Physics of Plasmas* **16**, 056309.

Stoeckl C, Boehly TR, Delettrez JA, Hatchett SP, Frenje JA, Glebov VY, Li CK, Miller JE, Petrasso RD, Séguin FH, Smalyuk VA, Stephens RB, Theobald W, Yaakobi B and Sangster TC (2005) Direct-drive fuel-assembly experiments with gas-filled, cone-in-shell, fast-ignitor targets on the OMEGA Laser. *Plasma Physics and Controlled Fusion* **47**, B859–B867.

Stoeckl C, Cruz M, Glebov VY, Knauer JP, Lauck R, Marshall K, Mileham C, Sangster TC and Theobald W (2010) A gated liquid-scintillator-based neutron detector for fast-ignitor experiments and down-scattered neutron measurements. *Review of Scientific Instruments* **81**, 10D302.

Tabak M, Hammer J, Glinsky ME, Kruer WL, Wilks SC, Woodworth J, Campbell EM and Perry MD (1994) Ignition and high gain with ultrapowerful lasers. *Physics of Plasmas* **1**, 1626–1634.

Theoobald W, Solodov AA, Stoeckl C, Anderson KS, Betti R, Boehly TR, Craxton RS, Delettrez JA, Dorrer C, Frenje JA, Glebov VY, Habara H, Tanaka KA, Knauer JP, Lauck R, Marshall FJ, Marshall KL, Meyerhofer DD, Nilson PM, Patel PK, Chen H, Sangster TC, Seka W, Sinenian N, Ma T, Beg FN, Giraldez E and Stephens RB (2011) Initial cone-in-shell fast-ignition experiments on OMEGA. *Physics of Plasmas* **18**, 056305.

Wu XC, Li RR, Peng TP, Zhang JH and Guo HS (2006) Precise calibration of 14.1 MeV neutron sensitivity of scintillator detector. *Nuclear Electron Detection Technologies* **26**, 710–713.

Zhu TH, Liu R, Jiang L, Lu XX, Wen ZW, Wang M and Lin JF (2007) The associated proton monitoring technique study of D-D source neutron yields at the large angle. *Nuclear Electron Detection Technologies* **27**, 141–144.

Zhu JQ, Zhu J, Li XC, Zhu BQ, Ma WX, Liu D, Liu C, Lu XQ, Fan W and Liu ZG (2017) High power glass laser research progresses in NLHPLP. Conference High power glass laser research progresses in NLHPLP, pp. 1008405.

https://doi.org/10.1017/S026303461800054X Published online by Cambridge University Press